THE JOURNAL OF PHYSICAL CHEMISTRY Letters

Letter

pubs.acs.org/JPCL

Charge Carrier Lifetimes Exceeding 15 μs in Methylammonium Lead Iodide Single Crystals

Yu Bi,[†,§] Eline M. Hutter,[†,§] Yanjun Fang,[‡] Qingfeng Dong,[‡] Jinsong Huang,[*,‡] and Tom J. Savenije[*,†]

[†]Optoelectronic Materials Section, Department of Chemical Engineering, Delft University of Technology, 2628 BL Delft, The Netherlands

[‡]Department of Mechanical and Materials Engineering and Nebraska Center for Materials and Nanoscience, University of Nebraska—Lincoln, Nebraska 68588-0656, United States

Supporting Information

ABSTRACT: The charge carrier lifetime in organic−inorganic perovskites is one of the most important parameters for modeling and design of solar cells and other types of devices. In this work, we use $CH_3NH_3PbI_3$ single crystal as a model system to study optical absorption, charge carrier generation, and recombination lifetimes. We show that commonly applied photoluminescence lifetime measurements may dramatically underestimate the intrinsic carrier lifetime in $CH_3NH_3PbI_3$, which could be due to severe charge recombination at the crystal surface and/or fast electron−hole recombination close to the surface. By using the time-resolved microwave conductivity technique, we investigated the lifetime of free mobile charges inside the crystals. Most importantly, we find that for homogeneous excitation throughout the crystal, the charge carrier lifetime exceeds 15 μs. This means that the diffusion length in $CH_3NH_3PbI_3$ can be as large as 50 μm if it is no longer limited by the dimensions of the crystallites.

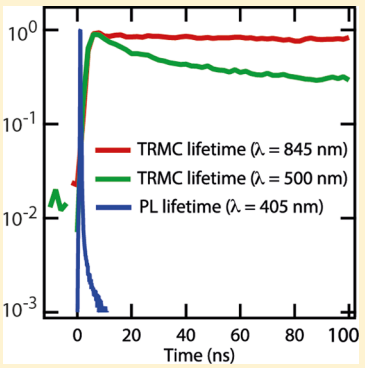

Organic−inorganic metal halide perovskites (OMHPs) are intensively investigated because these materials can be used as a photoactive layer in solar cells reaching efficiencies up to 20%.[1−11] Although there are many studies focusing on the material preparation, assembly, and characterization of OMHP solar cells, there is limited information on the generation of charges by photoexcitation and collection of charges by the electrodes. The relationship between the structure of the material, presence of dopants or grain boundaries, and the charge carrier dynamics is unclear. In particular, it is unknown to what extent the grain boundaries affect the charge carrier lifetime. This carrier lifetime determines the charge carrier diffusion length (L_D), which delineates the optimal thickness of the perovskite photoactive layer.[10,12] In previous studies on the diffusion length in perovskites, reported L_D values were limited by the dimensions of the thin films.[13−15] It has been shown that the material surface and grain boundaries impose a limitation to L_D in the case that the charge recombination inside the grains is negligible.[12,16] Direct visualization of the carrier density by transient absorption microscopy revealed a 2−8 fold longer lifetime in $CH_3NH_3PbI_3$ ($MAPbI_3$) polycrystalline films than in thin films with smaller crystallites and underscored the importance of material morphology in controlling the charge transport in (polycrystalline) thin films.[17,18] Recently, synthetic procedures have been developed to prepare large OMHP single crystals with sizes in excess of several millimeters, and in some case several centimeters.[19−23] These crystals form an ideal platform for investigating intrinsic material properties such as the charge carrier generation yield and lifetime. Initial studies on the charge carrier lifetimes in $MAPbI_3$ and $MAPbBr_3$ single crystals show a large variation, which might be attributed to the different measuring techniques. However, reported values for single crystals were all longer than those measured in thin films.[23−25] Additionally, electronic measurements, including transient photovoltaic and impedance spectroscopy, gave carrier lifetimes substantially longer (>100 μs) than optical measurements such as time-resolved photoluminescence (TRPL) (<0.1 μs).

Here, we study and compare charge carrier lifetimes in $MAPbI_3$ single crystals with dimensions of 10 × 8 × 3 mm^3, using the time-resolved microwave conductance (TRMC) technique and TRPL. With TRMC all photoinduced, mobile carriers generated in the crystal using a short laser pulse are probed. This technique allows us to monitor the photoinduced charge carrier formation and decay from 3 ns up to many microseconds. To investigate the effect of the surface on the charge carrier lifetime, we used different excitation wavelengths thereby varying the penetration depth. The latter parameter is a measure of how deep light penetrates into the perovskite crystal and is defined as the distance at which the light intensity inside the material falls to 1/e of the value at the surface. In this way, the location where the carriers are formed can be extensively manipulated (see Scheme 1).

$MAPbI_3$ single crystals were grown in a supersaturated $MAPbI_3$ precursor solution using the top-seeded-solution-growth method as described in previous work.[15] To obtain

Received: February 6, 2016
Accepted: February 22, 2016
Published: February 22, 2016

DOI: 10.1021/acs.jpclett.6b00269
J. Phys. Chem. Lett. 2016, 7, 923−928

Scheme 1. Overview of Photoinduced TRMC Technique[a]

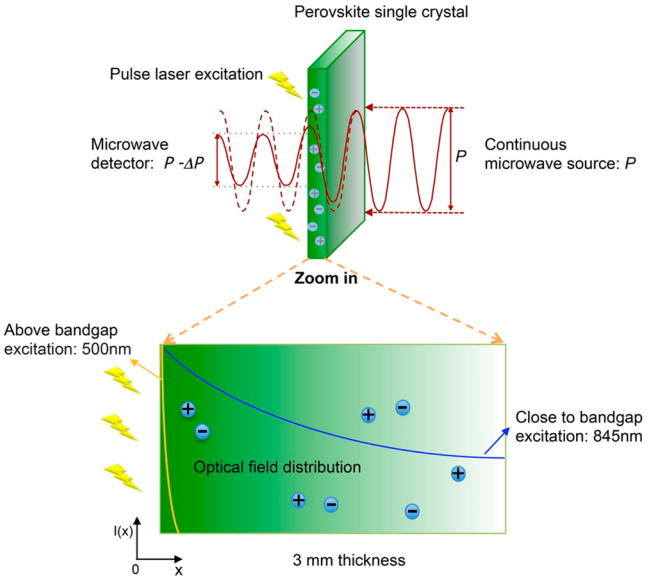

[a]Schematic representation of the TRMC measurement, where part of the incident microwave is absorbed because of charges generated in the perovskite crystal. This leads to a reduction of the amount of microwave power (P) measured by the detector. The expanded view of the sample depicts the charge carrier generation profile within the crystal upon excitation at 500 and 845 nm.

the wavelength-dependent penetration depth of the thick perovskite single crystal, the absorption spectrum, especially close to the bandgap, needs to be accurately determined. However, the absorption spectrum cannot be obtained by the common one-pass transmittance and reflectance measurements because of strong scattering (Figure 1A). Here we used an integrating sphere to collect both specular and diffuse reflectance, and by subtracting them from the incident light intensity we are able to get the absorption spectrum of the single crystal (Figure 1B). The absorption coefficient (α), which is equal to the reciprocal of the penetration depth, was further calculated by the following expression:

$$\frac{T_S + T_d}{100\% - R_S - R_d} = e^{-\alpha d} \quad (1)$$

where T_s is the specular transmittance, T_d the diffuse transmittance, R_s the specular reflectance, R_d the diffuse reflectance, and d the crystal thickness. From the wavelength-dependent absorption coefficient, shown in Figure 1B, we can derive that using an excitation wavelength of 500 nm the predominant part of the charges are generated within less than 100 nm of the surface. Using 845 nm light, which is close to the absorption onset as shown in Figure 1B, a homogeneous concentration profile is realized because the penetration depth, which amounts to 0.33 cm, is close to the thickness of 3 mm of the crystal.

Figure 2 shows the TRMC kinetics of the $MAPbI_3$ crystal expressed as the intensity-normalized change in absorbed microwave power ($\Delta P/PI_0$) in time. For both excitation wavelengths, i.e., 845 and 500 nm (panels A and B of Figure 2, respectively) the fast rise of the TRMC signal, which originates from the formation of mobile charges, is followed by a decay. This decay can be attributed to charge recombination or immobilization of the charge carriers by, for example, trapping. In Figure 2C we plotted the maximum signal sizes as a function of the photon fluence at different excitation wavelengths (500, 600, 800, and 845 nm), showing somewhat smaller values for the visible wavelengths (500 and 600 nm). In Figure 2D, the half lifetime, $\tau_{1/2}$ values are plotted versus incident intensity. Interestingly, on excitation at 845 nm, values of $\tau_{1/2}$ over 15 μs are found at low intensities ($<10^{12}$ photons per cm^2). However, upon increasing the intensity, the $\tau_{1/2}$ reduces down to about 100 ns. These light intensity-dependent carrier lifetimes explain the close to 100% internal quantum efficiency observed previously under weak excitation conditions in incident photon-to-current efficiency (IPCE) measurements, while lower efficiencies were obtained under higher excitation conditions, i.e., 1 sun illumination.[15] Note that charge carrier concentrations in the order of 10^{15} cm^{-3} are typical for steady-state AM1.5 solar radiation conditions.[26] For excitation at 500 and 600 nm, $\tau_{1/2}$ values show a reduction from a few hundreds of nanoseconds down to about 15 ns on increasing intensities. From these reductions in lifetimes for all wavelengths we can conclude that second-order (bimolecular) recombination reduces the photoconductance lifetime tremendously, which has been reported previously for both thin films and single crystals of this type of materials.[24,27−29] The reduction of the maximum signal sizes on higher intensities in Figure 2C are in line with this conclusion. Upon close inspection of the TRMC traces recorded on excitation at 500 nm (Figure 2B), we notice that in particular at higher intensities a small additional peak can be discerned within the first tens of nanoseconds, which is absent for excitation at 845 nm. This strong decay can be explained in two ways: (i) As mentioned above, we expect fast second-order recombination due to the high photoinduced charge carrier concentration (10^{17} cm^{-3}). (ii) In addition, strong charge recombination at the surface of the single crystals might occur. In the case that the surface of the crystal acts as an

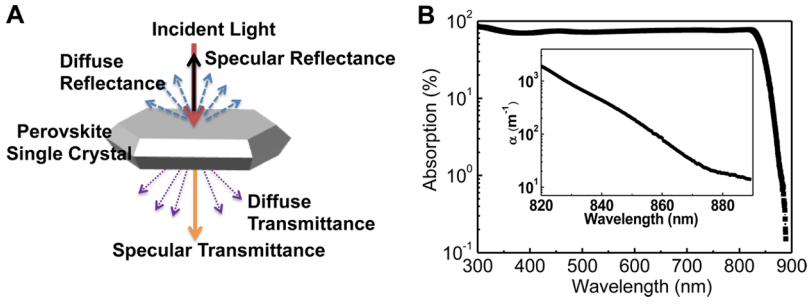

Figure 1. Optical absorption measurement. (A) Overview of the absorption spectrum measurement method of the $MAPbI_3$ single crystal. (B) The measured absorption spectrum and the corresponding absorption coefficient of the perovskite single crystal.

DOI: 10.1021/acs.jpclett.6b00269
J. Phys. Chem. Lett. 2016, 7, 923−928

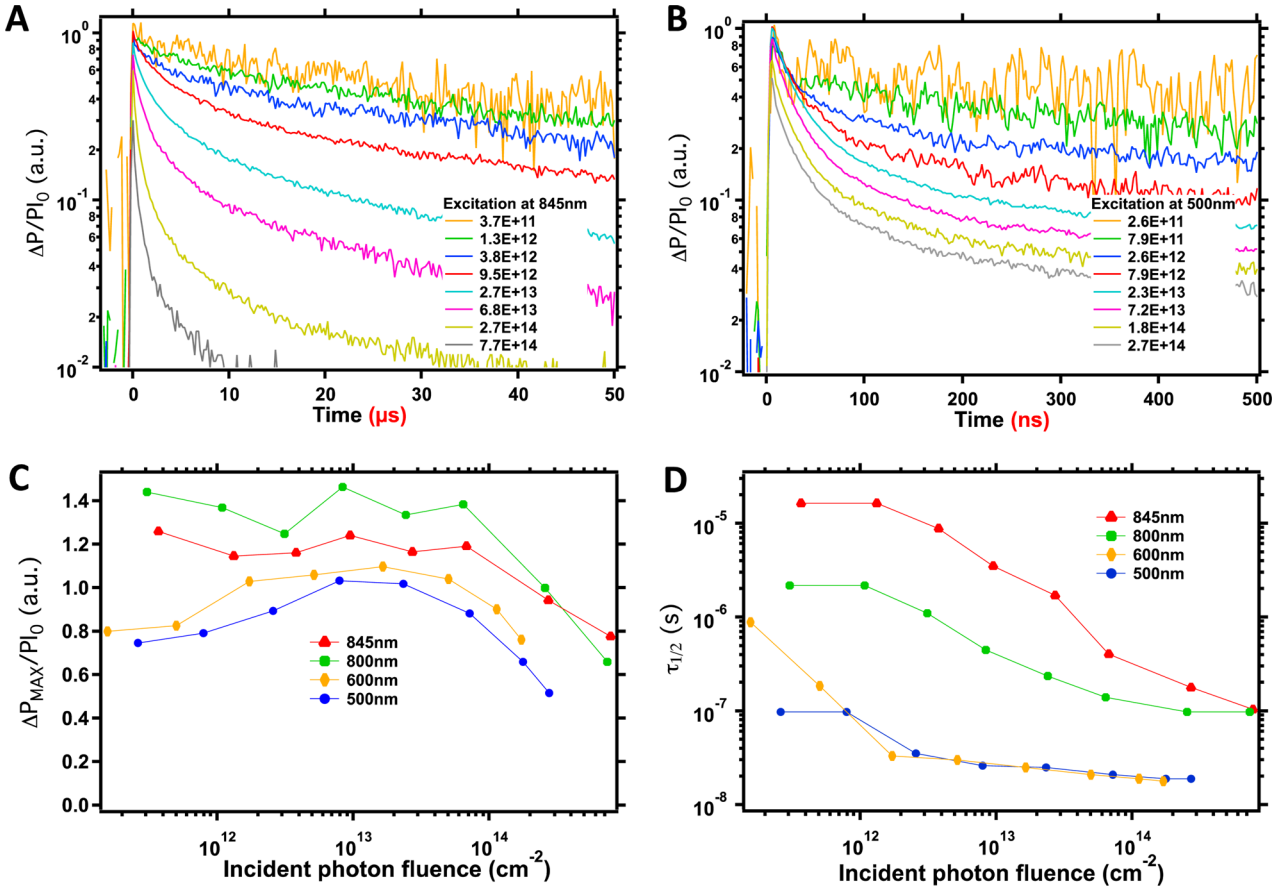

Figure 2. TRMC results under different excitation wavelengths and intensities. TRMC traces normalized to the incident intensity for the perovskite crystal recorded at excitation wavelengths of (A) 845 nm and (B) 500 nm using different indicated excitation intensities (photons/cm^2). Note that the horizontal scales are different. (C) Maximum change in normalized microwave power corrected for the amount of absorbed photons and (D) corresponding half lifetimes as a function of the photon fluence at indicated wavelengths.

efficient recombination site, one would expect a smaller signal size on optical excitation at 500 and 600 nm in agreement, with the observations shown in Figure 2C. For these wavelengths the largest part of the charge carriers is generated within 100 nm of the surface. Assuming a modest charge carrier mobility of 10 cm^2/(V s), these carriers have definitely encountered the crystal surface within a few nanoseconds, partially contributing to this fast initial decay. The absence of this fast decaying feature at 800 and 845 nm is consistent with the fact that, at this wavelength, most photoinduced carriers are generated further from the interface.

To find out the charge recombination channels in the single crystals, we applied a kinetic model, which was recently developed by us to describe the charge carrier dynamics in perovskite thin films.[29] To fit both the photoluminescence (PL) and TRMC lifetimes properly, a low concentration of electron traps in the perovskite films had to be assumed. This means that, on optical excitation, conduction band (CB) electrons are formed, which rapidly immobilize in these electron traps. The corresponding holes can contribute to the photoconductance until the trapped electrons recombine with the valence band holes. In case the number of CB electrons exceeds the number of electron traps by using higher excitation intensities, charge carrier decay kinetics are typically dominated by band-to-band recombination.[29,30] By using an excitation wavelength of 845 nm, the generated charge carriers are nearly homogeneously distributed throughout the crystals, because the penetration depth is close to the thickness of the crystals (see Scheme 1). Using the above model to fit the TRMC decay kinetics obtained at 845 nm with the fitting curves shown in Figure 3A, a very low trap concentration (N_T) of 1.5×10^{13} cm^{-3} is found in combination with a second-order recombination rate (k_2) of 5.5×10^{-9} cm^3 s^{-1} (see Supporting Information for more information regarding the kinetic model). It is important to mention here that all traces shown in Figure 3A recorded using intensities varying over 3 orders of magnitude could be satisfactorily fitted with these parameters. Interestingly, N_T is at least 1 order of magnitude lower than values found in $MAPbI_3$ thin films.[29−32] This discrepancy could be attributed to the lack of grain boundaries within the single crystals. Furthermore, the k_2 is about 1 order of magnitude higher than reported in several kinetic studies.[29−32] We suggest that the higher charge carrier mobility caused by the superior crystallinity in the crystal results in an enhancement of k_2.

Next, we use the above values for N_T and k_2 to calculate the TRMC traces for excitation at 500 nm using the corresponding absorption coefficient. As shown in the Supporting Information information (see Figure S1), the calculated traces decay much faster than those observed experimentally. Obviously, recombination is retarded for charge carriers generated at high concentrations using this wavelength. From this we deduce that it is likely that due to the high initial charge carrier concentration gradient, carriers diffuse toward the bulk of the

DOI: 10.1021/acs.jpclett.6b00269
J. Phys. Chem. Lett. 2016, 7, 923−928

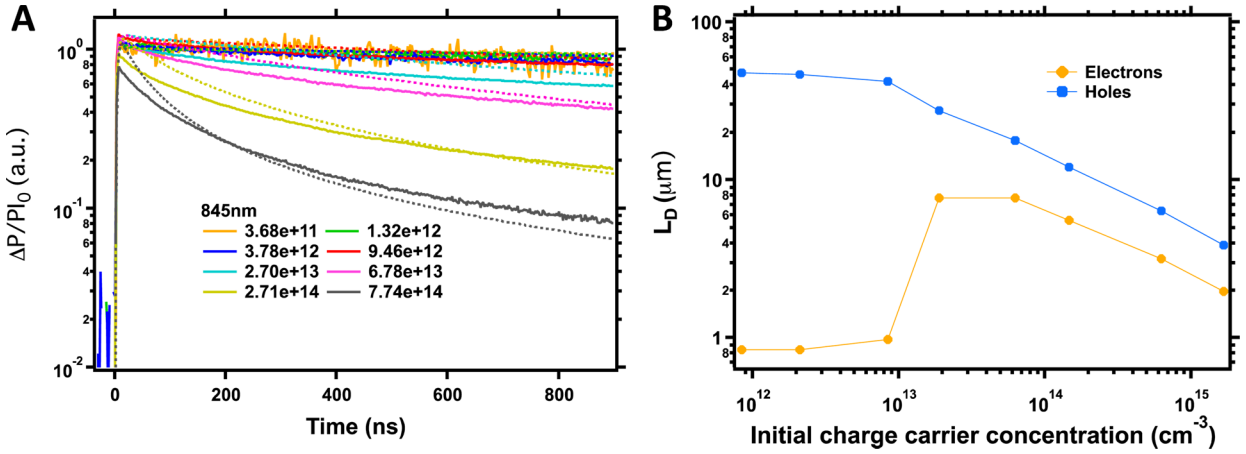

Figure 3. Analysis of TRMC data. (A) Fits (dashed lines) to the TRMC traces (full lines) using the model as described in the text for excitation at 845 nm, where charges are generated homogeneously throughout the crystal. (B) Logarithmic plot of the diffusion length for majority carriers (holes, blue) and minority carriers (electrons, yellow) as a function of the concentration of photoexcited charge carriers.

crystal leading to lowered concentrations and hence longer lifetimes.

TRMC signals originate both from mobile electrons and mobile holes. Thus, the recorded TRMC lifetimes may be dominated by one of these two charges, especially in the excitation regime where the electrons are immobilized in an intraband gap state. However, the kinetic model enables us to distinguish between the contributions of electrons and holes, and consequently, the lifetimes can be separated (see Figure S2). This shows that at low light intensities, the hole lifetime (microseconds) is much longer than the electron lifetime (<50 ns). On the other hand, when the concentration of photoexcited electrons exceeds the number of trap states, the electron lifetime can be in the order of microseconds as well. In this higher excitation regime, both the electron and hole lifetimes are dominated by second-order recombination rates. As a consequence, the charge carrier diffusion length is highly dependent on the excitation energy. Figure 3B shows the electron (minority carrier) and hole (majority carrier) diffusion lengths as a function of the initial concentration of photogenerated electron−hole pairs. Distances were calculated with $L_D = \sqrt{\frac{kT}{e}\mu\tau_{1/2}}$, using the half lifetimes from Figure S2 and the electron and hole mobilities previously reported for this type of single crystals.[20]

These results show that below the trap concentration (<1.5 × 10^{13} cm^{-3}), the electron diffusion length is 0.8 μm, which increases to 8 μm just above the trap concentration. For the holes, the diffusion length reaches a maximum value of 50 μm, which is attributed to the slow recombination with a trapped electron.[29,30] At higher concentrations, the diffusion lengths of both electrons and holes reduce because of increasing second-order electron−hole recombination. Probably, the observed trend in Figure 3B can be generalized to thin perovskite films: the diffusion lengths will be optimal at an electron−hole concentration just above the trap density. Note that these results apply to a homogeneous, pulsed excitation profile; additional diffusion resulting from a concentration gradient is not taken into account.

PL measurements were performed on the same single crystal, and the spectrum is shown in the inset revealing the emission spectrum of the $MAPbI_3$. Interestingly, the PL kinetics shown in Figure 4 are substantially faster than the TRMC decays. The

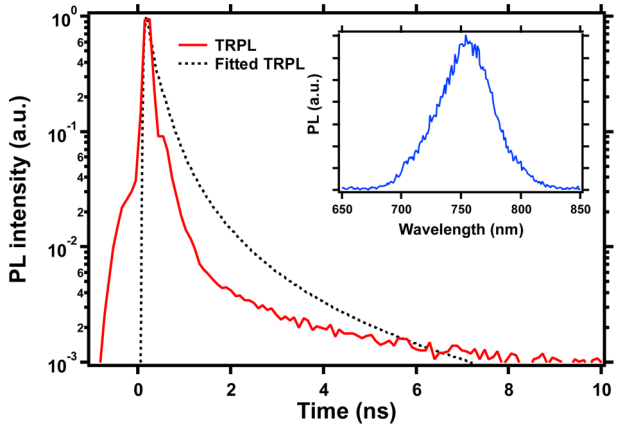

Figure 4. Time-resolved photoluminescence. TRPL trace of single-crystal perovskite on pulsed excitation at 405 nm with an intensity of 4 × 10^{12} photons cm^{-2}, detected at 760 nm (dashed line) and PL trace calculated with the model described in the text (full line). The inset shows the emission spectrum of the single-crystal $MAPbI_3$ using an excitation wavelength of 405 nm.

$\tau_{1/2}$ value is about a nanosecond, which is comparable to previously published values.[24] For this decay, the excitation wavelength is 405 nm, which yields a very high surface concentration of charge carriers, which undergo rapid band-to-band recombination leading to the fast decay kinetics. Next, using the same parameters for N_T and k_2 found for fitting the TRMC traces at 845 nm and the appropriate value for the absorption coefficient at 405 nm, a TRPL trace is calculated as described previously and added in Figure 4.[29] For the calculated PL trace, only the emission of the surface layer with a thickness of half the penetration depth is taken into account. PL emitted more in the interior of the crystal is likely to be reabsorbed and will therefore not be probed.[24] Interestingly, the measured PL decay is close to the calculated trace. Additional surface recombination might explain the remaining small difference between the calculated and measured PL.

Altogether, these results show that the short PL lifetimes, as typically observed for single crystals, can be explained by the relatively high recombination rate, k_2, in combination with the high concentration of charge carriers recombining radiatively close to the surface of the crystal. Hence, the differences

DOI: 10.1021/acs.jpclett.6b00269
J. Phys. Chem. Lett. 2016, 7, 923−928

observed in the decay kinetics for the single crystal using PL and TRMC highlight the dissimilarities in measuring techniques. While PL probes only radiative recombination close to the surface, TRMC probes all mobile carriers formed within the crystal. From this it can be deduced that for single crystals, the PL lifetimes are not representative of the lifetime of free mobile charges within the crystal and therefore are not suitable to determine the charge carrier diffusion lengths. Instead of $\tau_{1/2}$ values of several nanoseconds as found by TRPL, TRMC reveals that under low excitation energies ($<10^{12}$ photons per cm^2), $\tau_{1/2}$ can be as large as 15 μs. This value exceeds the lifetime of carriers in similar crystals found by, for example, two-photon excitation.[24]

In summary, we used different techniques to study the optical absorption, charge carrier generation, and recombination lifetimes in $CH_3NH_3PbI_3$ single crystals. The absorption coefficient of light in a single crystal was determined using an integrating sphere. The corresponding penetration depths were used to manipulate the location of charge generation: while excitation at 845 nm results in a homogeneous concentration profile, excitation in the visible leads to charge carrier generation predominantly within 100 nm of the surface. Using the TRMC technique, we found that the maximum photoconductance upon excitation in the visible is somewhat smaller than those obtained near the band gap. Interestingly, excitation at 845 nm results in $\tau_{1/2}$ values over 15 μs at low intensities ($<10^{12}$ photons per cm^2). On the other hand, when the intensity is increased, $\tau_{1/2}$ reduces to about 100 ns. From fitting a kinetic model to the TRMC decay kinetics obtained at 845 nm, a very low trap concentration of 1.5×10^{13} cm^{-3} is deduced in combination with a second-order recombination rate of 5.5×10^{-9} cm^3 s^{-1}. These results show that the diffusion length can reach distances up to 50 μm. This is mainly due to the microsecond lifetimes of mobile charge carriers in these single crystals, which is in contrast with the PL lifetime of less than 10 ns. However, because PL probes only radiative recombination close to the surface and TRMC probes all mobile carriers formed within the crystal, we conclude that PL lifetimes are not representative for the lifetime of free mobile charges within the crystal and are not appropriate for determining the charge carrier diffusion lengths.

EXPERIMENTAL SECTION

Crystal Synthesis. A mixture of 29.3 g of lead(II) acetate trihydrate, 120 mL of hydriodic acid (HI) (57% w/w aq soln), and 5.97 g of methylamine (CH_3NH_2) (40% w/w aq soln) was heated to 100 °C until the precursors were fully dissolved. Then, the mixture was cooled to 75 °C for pacification of small $MAPbI_3$ crystals. The clear blend solution was transferred to a closed container with a silicon substrate, inserted on top of the solution. The small crystals were introduced at the bottom of the container as raw materials for crystal growth. The container was placed in an oil bath of 75 °C, where the bottom was immersed in the oil and the top exposed to air. The $MAPbI_3$ single crystals nucleated on the silicon substrate were used as seeds for further growth to large single crystals. Finally, the as-grown single crystals were washed with diethyl ether and dried in vacuum.

Optical Measurements. The absorption measurement of the single crystal was performed on a LAMBDA 1050 UV/vis/NIR spectrophotometer (PerkinElmer) equipped with an integrating sphere. Photoluminescence emission spectra and PL lifetimes were recorded using an Edinburgh LifeSpec spectrometer using time-correlated single photon counting. The $MAPbI_3$ crystal was excited at 405 nm with a picosecond pulsed diode laser (Hamamatsu, M8903-01, $I_0 = 4 \times 10^{12}$ photons/cm^2).

Photoconductance Measurements. A $MAPbI_3$ single crystal was glued on a quartz substrate and mounted in a sealed microwave cell within an N_2-filled glovebox. The time-resolved microwave conductivity technique was used to measure the change in microwave (ca. 11 GHz) power on pulsed optical excitation of the $MAPbI_3$ single crystal.[33] The photoinduced normalized change in microwave power ($\Delta P/P$) is corrected for the number of incident photons (I_0) to allow comparison with other wavelengths. The rise of $\Delta P/P$ is limited by the width of the laser pulse (3.5 ns fwhm) and the response time of our microwave system (1−2 ns). The slow repetition rate of the laser of 10 Hz ensures full relaxation of all photoinduced charges to the ground state. During the TRMC measurements, the samples were not exposed to moisture and air to prevent any degradation.

ASSOCIATED CONTENT

Supporting Information

The Supporting Information is available free of charge on the ACS Publications website at DOI: 10.1021/acs.jpclett.6b00269.

SEM, XRD, and additional TRMC data (PDF)

AUTHOR INFORMATION

Corresponding Authors

*E-mail: T.J.Savenije@tudelft.nl.

*E-mail: jhuang2@unl.edu.

Author Contributions

§Y.B. and E.M.H. contributed equally to this work.

Notes

The authors declare no competing financial interest.

ACKNOWLEDGMENTS

Y.B., E.M.H., and T.J.S. thank NWO and STW for funding. Y.F., Q.D., and J.H. acknowledge financial support from National Science Foundation under Award OIA-1538893.

REFERENCES

(1) Im, J.-H.; Jang, I.-H.; Pellet, N.; Grätzel, M.; Park, N.-G. Growth of CH3NH3PbI3 Cuboids with Controlled Size for High-Efficiency Perovskite Solar Cells. *Nat. Nanotechnol.* **2014**, *9* (11), 927−932.

(2) Zhou, H.; Chen, Q. Q.; Li, G.; Luo, S.; Song, T. T.-B.; Duan, H.-S. H.-S.; Hong, Z.; You, J.; Liu, Y.; Yang, Y. Interface Engineering of Highly Efficient Perovskite Solar Cells. *Science* **2014**, *345*, 542−546.

(3) Burschka, J.; Pellet, N.; Moon, S.-J.; Humphry-Baker, R.; Gao, P.; Nazeeruddin, M. K.; Grätzel, M. Sequential Deposition as a Route to High-Performance Perovskite-Sensitized Solar Cells. *Nature* **2013**, *499* (7458), 316−319.

(4) National Renewable Energy Laboratory. http://www.nrel.gov.

(5) Green, M. A.; Ho-Baillie, A.; Snaith, H. J. The Emergence of Perovskite Solar Cells. *Nat. Photonics* **2014**, *8* (7), 506−514.

(6) McGehee, M. D. Perovskite Solar Cells: Continuing to Soar. *Nat. Mater.* **2014**, *13*, 845−846.

(7) Noel, N. K.; Abate, A.; Stranks, S. D.; Parrott, E. S.; Burlakov, V. M.; Goriely, A.; Snaith, H. J. Enhanced Photoluminescence and Solar Cell Performance via Lewis Base Passivation of Organic-Inorganic Lead Halide Perovskites. *ACS Nano* **2014**, *8* (10), 9815−9821.

(8) Deng, Y.; Peng, E.; Shao, Y.; Xiao, Z.; Dong, Q.; Huang, J. Scalable Fabrication of Efficient Organolead Trihalide Perovskite Solar Cells with Doctor-Bladed. *Energy Environ. Sci.* **2015**, *8*, 1544−1550.

DOI: 10.1021/acs.jpclett.6b00269
J. Phys. Chem. Lett. 2016, 7, 923−928

(9) Jeon, N. J.; Noh, J. H.; Yang, W. S.; Kim, Y. C.; Ryu, S.; Seo, J.; Seok, S. Il. Compositional Engineering of Perovskite Materials for High-Performance Solar Cells. *Nature* **2015**, *517*, 476−480.
(10) Stranks, S. D.; Snaith, H. J. Metal-Halide Perovskites for Photovoltaic and Light-Emitting Devices. *Nat. Nanotechnol.* **2015**, *10* (5), 391−402.
(11) Li, X.; Dar, M. I.; Yi, C.; Luo, J.; Tschumi, M.; Zakeeruddin, S. M.; Nazeeruddin, M. K.; Han, H.; Grätzel, M. Improved Performance and Stability of Perovskite Solar Cells by Crystal Crosslinking with Alkylphosphonic Acid W-Ammonium Chlorides. *Nat. Chem.* **2015**, *7*, 703−711.
(12) Huang, J.; Shao, Y.; Dong, Q. Organometal Trihalide Perovskite Single Crystals: A Next Wave of Materials for 25% Efficiency Photovoltaics and Applications Beyond? *J. Phys. Chem. Lett.* **2015**, *6* (16), 3218−3227.
(13) Xing, G.; Mathews, N.; Sun, S.; Lim, S. S.; Lam, Y. M.; Grätzel, M.; Mhaisalkar, S.; Sum, T. C. Long-Range Balanced Electron- and Hole-Transport Lengths in Organic-Inorganic CH3NH3PbI3. *Science* **2013**, *342* (6156), 344−347.
(14) Xiao, Z.; Bi, C.; Shao, Y.; Dong, Q.; Wang, Q.; Yuan, Y.; Wang, C.; Gao, Y.; Huang, J. Efficient, High Yield Perovskite Photovoltaic Devices Grown by Interdiffusion of Solution-Processed Precursor Stacking Layers. *Energy Environ. Sci.* **2014**, *7* (8), 2619.
(15) de Quilettes, D. W.; Vorpahl, S. M.; Stranks, S. D.; Nagaoka, H.; Eperon, G. E.; Ziffer, M. E.; Snaith, H. J.; Ginger, D. S. Impact of Microstructure on Local Carrier Lifetime in Perovskite Solar Cells. *Science* **2015**, *348* (6235), 683−686.
(16) Xiao, Z.; Dong, Q.; Bi, C.; Shao, Y.; Yuan, Y.; Huang, J. Solvent Annealing of Perovskite-Induced Crystal Growth for Photovoltaic-Device Effi Ciency Enhancement. *Adv. Mater.* **2014**, *26* (37), 6503−6509.
(17) Guo, Z.; Manser, J. S.; Wan, Y.; Kamat, P. V.; Huang, L. Spatial and Temporal Imaging of Long-Range Charge Transport in Perovskite Thin Films by Ultrafast Microscopy. *Nat. Commun.* **2015**, *6*, 7471.
(18) Tian, W.; Zhao, C.; Leng, J.; Cui, R.; Jin, S. Visualizing Carrier Diffusion in Individual Single-Crystal Organolead Halide Perovskite Nanowires and Nanoplates. *J. Am. Chem. Soc.* **2015**, *137* (39), 12458−12461.
(19) Dang, Y.; Liu, Y.; Sun, Y.; Yuan, D.; Liu, X.; Lu, W.; Liu, G.; Xia, H.; Tao, X. Bulk Crystal Growth of Hybrid Perovskite Material CH3NH3PbI3. *CrystEngComm* **2015**, *17* (3), 665−670.
(20) Dong, Q.; Fang, Y.; Shao, Y.; Mulligan, P.; Qiu, J.; Cao, L.; Huang, J. Electron-Hole Diffusion Lengths > 175 μm in Solution-Grown CH3NH3PbI3 Single Crystals. *Science* **2015**, *347* (6225), 967−970.
(21) Saidaminov, M. I.; Abdelhady, A. L.; Murali, B.; Alarousu, E.; Burlakov, V. M.; Peng, W.; Dursun, I.; Wang, L.; He, Y.; Maculan, G.; et al. High-Quality Bulk Hybrid Perovskite Single Crystals within Minutes by Inverse Temperature Crystallization. *Nat. Commun.* **2015**, *6*, 7586.
(22) Fang, Y.; Dong, Q.; Shao, Y.; Yuan, Y.; Huang, J. Highly Narrowband Perovskite Single-Crystal Photodetectors Enabled by Surface-Charge Recombination. *Nat. Photonics* **2015**, *9* (10), 679−686.
(23) Shi, D.; Adinolfi, V.; Comin, R.; Yuan, M.; Alarousu, E.; Buin, A.; Chen, Y.; Hoogland, S.; Rothenberger, A.; Katsiev, K.; et al. Low Trap-State Density and Long Carrier Diffusion in Organolead Trihalide Perovskite Single Crystals. *Science* **2015**, *347* (6221), 519−522.
(24) Yamada, Y.; Yamada, T.; Phuong, L. Q.; Maruyama, N.; Nishimura, H.; Wakamiya, A.; Murata, Y.; Kanemitsu, Y. Dynamic Optical Properties of CH3NH3PbI3 Single Crystals As Revealed by One- and Two-Photon Excited Photoluminescence Measurements. *J. Am. Chem. Soc.* **2015**, *137* (33), 10456−10459.
(25) Fang, H. H.; Raissa, R.; Abdu-Aguye, M.; Adjokatse, S.; Blake, G. R.; Even, J.; Loi, M. A. Photophysics of Organic-Inorganic Hybrid Lead Iodide Perovskite Single Crystals. *Adv. Funct. Mater.* **2015**, *25* (16), 2378−2385.
(26) Johnston, M. B.; Herz, L. M. Hybrid Perovskites for Photovoltaics: Charge-Carrier Recombination, Diffusion, and Radiative Efficiencies. *Acc. Chem. Res.* **2016**, *49*, 146.
(27) Savenije, T. J.; Ponseca, C. S., Jr.; Kunneman, L.; Abdellah, M.; Zheng, K.; Tian, Y.; Zhu, Q.; Canton, S. E.; Scheblykin, I. G.; Pullerits, T.; et al. Thermally Activated Exciton Dissociation and Recombination Control the Carrier Dynamics in Organometal Halide Perovskite. *J. Phys. Chem. Lett.* **2014**, *5*, 2189−2194.
(28) Ponseca, C. S.; Savenije, T. J.; Abdellah, M.; Zheng, K.; Yartsev, A.; Pascher, T.; Harlang, T.; Chabera, P.; Pullerits, T.; Stepanov, A.; et al. Organometal Halide Perovskite Solar Cell Materials Rationalized: Ultrafast Charge Generation, High and Microsecond-Long Balanced Mobilities, and Slow Recombination. *J. Am. Chem. Soc.* **2014**, *136* (14), 5189−5192.
(29) Hutter, E. M.; Eperon, G. E.; Stranks, S. D.; Savenije, T. J. Charge Carriers in Planar and Meso-Structured Organic-Inorganic Perovskites: Mobilities, Lifetimes and Concentrations of Trap States. *J. Phys. Chem. Lett.* **2015**, *6*, 3082−3090.
(30) Stranks, S. D.; Burlakov, V. M.; Leijtens, T.; Ball, J. M.; Goriely, A.; Snaith, H. J. Recombination Kinetics in Organic-Inorganic Perovskites: Excitons, Free Charge, and Subgap States. *Phys. Rev. Appl.* **2014**, *2* (3), 034007.
(31) Wehrenfennig, C.; Eperon, G. E.; Johnston, M. B.; Snaith, H. J.; Herz, L. M. High Charge Carrier Mobilities and Lifetimes in Organolead Trihalide Perovskites. *Adv. Mater.* **2014**, *26* (10), 1584−1589.
(32) Wehrenfennig, C.; Liu, M.; Snaith, H. J.; Johnston, M. B.; Herz, L. M. Charge-Carrier Dynamics in Vapour-Deposited Films of the Organolead Halide Perovskite CH3NH3PbI3−xClx. *Energy Environ. Sci.* **2014**, *7*, 2269−2275.
(33) Savenije, T. J.; Ferguson, A. J.; Kopidakis, N.; Rumbles, G. Revealing the Dynamics of Charge Carriers in Polymer:fullerene Blends Using Photoinduced Time-Resolved Microwave Conductivity. *J. Phys. Chem. C* **2013**, *117* (46), 24085−24103.

DOI: 10.1021/acs.jpclett.6b00269
J. Phys. Chem. Lett. 2016, 7, 923−928